Nuclear Engineering and Technology 55 (2023) 1527–1532

Contents lists available at ScienceDirect

Nuclear Engineering and Technology

journal homepage: www.elsevier.com/locate/net

Original Article

Experimental study of noise level optimization in brain single-photon emission computed tomography images using non-local means approach with various reconstruction methods

Seong-Hyeon Kang [a, b], Seungwan Lee [c, *], Youngjin Lee [d, **]

[a] Department of Health Science, General Graduate School of Gachon University, Republic of Korea
[b] Department of Biomedical Engineering, Eulji University, Republic of Korea
[c] Department of Radiological Science, Konyang University, Republic of Korea
[d] Department of Radiological Science, College of Health Science, Gachon University, Republic of Korea

ARTICLE INFO

Article history:
Received 11 October 2022
Received in revised form
28 December 2022
Accepted 15 January 2023
Available online 14 February 2023

Keywords:
Non-local means (NLM) approach
Noise reduction algorithm
Optimization of NLM algorithm
SPECT image reconstruction methods
Quantitative evaluation of image quality

ABSTRACT

The noise reduction algorithm using the non-local means (NLM) approach is very efficient in nuclear medicine imaging. In this study, the applicability of the NLM noise reduction algorithm in single-photon emission computed tomography (SPECT) images with a brain phantom and the optimization of the NLM algorithm by changing the smoothing factors according to various reconstruction methods are investigated. Brain phantom images were reconstructed using filtered back projection (FBP) and ordered subset expectation maximization (OSEM). The smoothing factor of the NLM noise reduction algorithm determined the optimal coefficient of variation (COV) and contrast-to-noise ratio (CNR) results at a value of 0.020 in the FBP and OSEM reconstruction methods. We confirmed that the FBP- and OSEM-based SPECT images using the algorithm applied with the optimal smoothing factor improved the COV and CNR by 66.94% and 8.00% on average, respectively, compared to those of the original image. In conclusion, an optimized smoothing factor was derived from the NLM approach-based algorithm in brain SPECT images and may be applicable to various nuclear medicine imaging techniques in the future.

1. Introduction

A representative device for nuclear medicine imaging is a gamma camera using a single energy-emitting nuclide, and single-photon emission computed tomography (SPECT), designed to acquire three-dimensional information, is used primarily to acquire more accurate lesion information [1,2]. One of the major problems with gamma cameras and SPECT images is that they generate more noise than radiographs. Because the noise in a medical image depends on the number of detected photons, the amount of noise in a nuclear medicine image inevitably increases [3]. SPECT images used for brain perfusion studies have various advantages compared to other modalities, but the noise generated in the area to be observed may reduce the accuracy of diagnosis [4]. *Nikolov* et al. reported that brain SPECT noise can cause very low cerebral blood flow values due to low perfusion and that the histogram of the acquired image may be deformed [5].

The reconstruction method is one of the most sensitive factors affecting noise in brain SPECT images. Filtered back projection (FBP) is the most widely used method to reconstruct SPECT images in nuclear medicine [6]. An indirect solution method is used through expectation maximization (EM) as an iterative reconstruction method, and the ordered subset EM (OSEM) method is most efficiently applied to SPECT image reconstruction [7]. Depending on the method of reconstructing the SPECT image, the image quality and noise characteristics are changed. According to the study by *Trevisan* et al., the OSEM reconstruction method was superior to the qualitative and quantitative evaluation results compared to the FBP and said that it would help prepare a brain SPECT image evaluation index for the diagnosis of Alzheimer's or Parkinson's disease [8].

A typical approach to reduce the noise in nuclear medicine images is to use software. Among these techniques, the non-local means (NLM) approach has proven effective in noise reduction since it was proposed by *Rudin* et al., in 1991, and its use has been

* Corresponding author. Department of Radiological Science, Konyang University, 158 Gwanjeodong-ro, Daejeon, 320-812, Republic of Korea.
** Corresponding author. Department of Radiological Science, Gachon University, 191, Hambakmoero, Yeonsu-gu, Incheon, Republic of Korea.
E-mail addresses: slee1@konyang.ac.kr (S. Lee), yj20@gachon.ac.kr (Y. Lee).

https://doi.org/10.1016/j.net.2023.01.013

increased by many researchers in medicine [9–12]. To observe the structural details in detail, a noise reduction algorithm using the NLM approach is actively applied to computed tomographs and magnetic resonance images [10,11]. *Jang* et al. showed the usefulness of the NLM noise reduction algorithm in SPECT images obtained using the OSEM reconstruction method based on the Hoffman 3D brain phantom and ^{99m}Tc radioisotope [12]. They confirmed that the quantitative noise level of the NLM noise reduction algorithm was significantly reduced compared to the Gaussian and median filters, which are previously used filtering methods.

The parameters that can be changed during the modeling of the NLM noise reduction algorithm affect the quality of the resulting image. Among these parameters, it is essential to derive an appropriate value of the smoothing factor with the greatest influence on the noise intensity control.

When an excessive smoothing factor is applied to the acquired image, an appropriate value must be determined, because noise and information about the area that needs to be observed may be lost. According to *Kang* et al., the smoothing factor of the NLM noise reduction algorithm in the color image was studied and as a result, a parameter of an appropriate level was derived [13]. However, few studies have been conducted to optimize the smoothing factor of the NLM noise reduction algorithm in SPECT images.

In this study, we attempted to derive the optimized smoothing factor of the NLM noise reduction algorithm in brain SPECT images using various reconstruction methods. Using a real SPECT system, we intend to apply the NLM noise reduction algorithm to various smoothing factors modeled and acquired from brain phantom images. As quantitative evaluation factors for optimization, we want to use the coefficient of variation (COV) and contrast-to-noise ratio (CNR) and to prove the usefulness of the proposed method by comparing the optimized SPECT image with conventional filtering-based images.

2. Materials and methods

2.1. Used SPECT imaging system and phantom

A dual-head detector-based SPECT imaging system using the Infinia Hawkeye 4 (GE Healthcare, Chicago, IL, USA) model was used. A 99mTc radioisotope (250 μCi) was used, and images were acquired at a frame rate of 3 s/frame with a parallel-hole collimator. For the reconstruction method, FBP and OSEM with two iterations and 10 subsets were used, and a Butterworth filter with 0.5 critical frequency and 10 power was applied to both. A Hoffman brain phantom was used.

2.2. Modeling of NLM noise reduction algorithm

The NLM approach has a great advantage in that it can show results similar to those obtained using multiple images by collecting similar areas within one image and then taking the average [9]. *Buades* et al. proposed a method to efficiently reduce image noise using this principle [14]. Theoretically, the NLM denoising algorithm is based on the following equation.

$$NL[\mathrm{v}(i)] = \sum_{j \in \Delta_i} w(i,j)v(j) \tag{1}$$

where $\mathrm{r}(i)$ and $r(j)$ denote the brightness of pixels i and the pixel j, respectively, Δ_i denotes a search volume set centered on pixel i, and $w(i,j)$ denotes a weight indicating the similarity between pixel i and pixel j. The $w(i,j)$ must satisfy $0 \leq w(i,j) \leq 1$, and in general, the amount of calculation is reduced when calculating the weights for neighboring pixels. The $w(i,j)$ can be calculated using the exponential function for the difference in the neighboring regions as follows:

$$w(i,j) = \frac{1}{Z_i} exp\left(- \frac{\left\| v(N_i) - v(N_j) \right\|_{2,a}^2}{h^2} \right) \tag{2}$$

where Z_i is a normalizing constant, h is a smoothing factor, and $v(N_i)$ and $v(N_j)$ are pixel vectors composed of neighboring pixels of two pixels i and j, respectively. In this study, the smoothing factor, which has a major influence on the noise level, was increased from 0.005 to 0.050 in steps of 0.005 and applied to the acquired SPECT image.

2.3. Quantitative evaluation of image quality

The COV and CNR parameters were used for the quantitative evaluation and optimization of the SPECT images acquired using the NLM noise reduction algorithm, to which various smoothing factors were applied. The two evaluation parameters were calculated using the following formula using the region of interest (ROI) in Fig. 1 [15].

$$\mathrm{COV} = \frac{\sigma_{\mathrm{Target}}}{S_{\mathrm{Target}}} \tag{3}$$

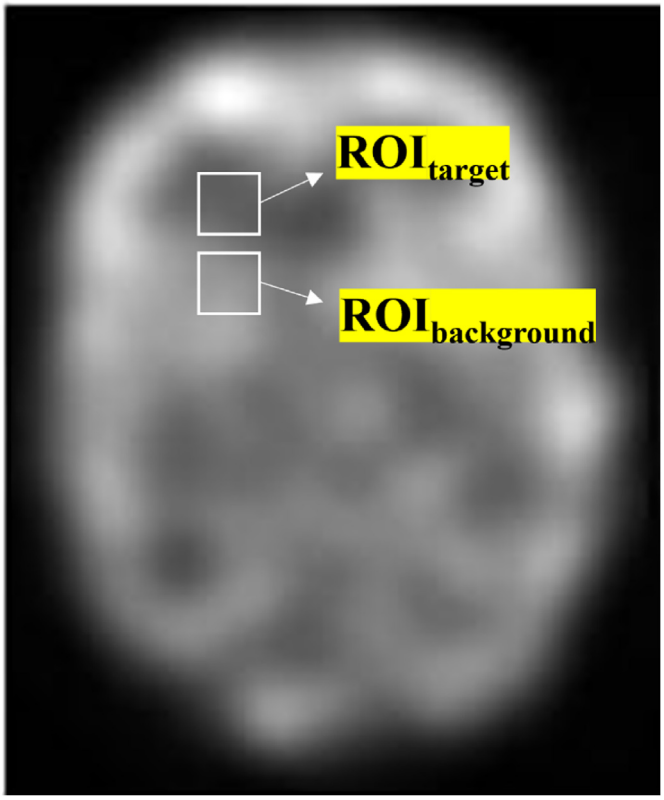

Fig. 1. Region of interest (ROI) set-up for COV and CNR evaluation in acquired sample SPECT images. $\mathrm{ROI}_{\mathrm{target}}$ was used for CNR and COV evaluation, and $\mathrm{ROI}_{\mathrm{background}}$ was used for CNR evaluation.

$$CNR = \frac{\left|S_{Target} - S_{Background}\right|}{\sqrt{\sigma_{Target}{}^2 + \sigma_{Background}{}^2}} \quad (4)$$

where S_{Target} and σ_{target} indicate the signal and standard deviation values in the target regions, respectively, $S_{Background}$ and $\sigma_{Background}$ represent the signal and standard deviation values in the background regions, respectively.

3. Results and discussion

Fig. 2 shows the results according to the change in the smoothing factor of the NLM noise reduction algorithm in the brain SPECT image using the FBP reconstruction method. Fig. 2 (a) shows a SPECT image obtained by changing the smoothing factor of the NLM noise reduction algorithm and shows a full-size image and an enlarged image of the brain area. In addition, graphs of the results of the COV and CNR according to the smoothing factor measured in Fig. 2 (a) images are shown in Fig. 2 (b) and (c), respectively. We confirmed that the COV result of the FBP reconstructed image gradually decreased as the smoothing factor increased. When using a smoothing factor of 0.005, the COV value was measured to be 0.0049 and was confirmed to be 0.0020 when using a smoothing factor of 0.050. When the NLM noise reduction algorithm using a smoothing factor of 0.020 was applied to the SPECT image, a COV of 0.0021 was derived, similar to the result measured at a smoothing factor of 0.050. In addition, we confirmed that the CNR results of the FBP reconstructed image gradually increased as the smoothing factor increased. When a smoothing factor of 0.005 was used, the CNR value was measured to be 15.89, which was confirmed to be 18.22 with a smoothing factor of 0.050. When the NLM noise reduction algorithm using a smoothing factor of 0.020 was applied to the SPECT image, a CNR of 17.79 was derived, similar to the result measured at a smoothing factor of 0.050. We proved that applying the NLM noise reduction algorithm with a smoothing factor of 0.020 to the brain SPECT image based on the FBP reconstruction method is the optimal value because the slope change of the COV and CNR result graphs becomes almost constant.

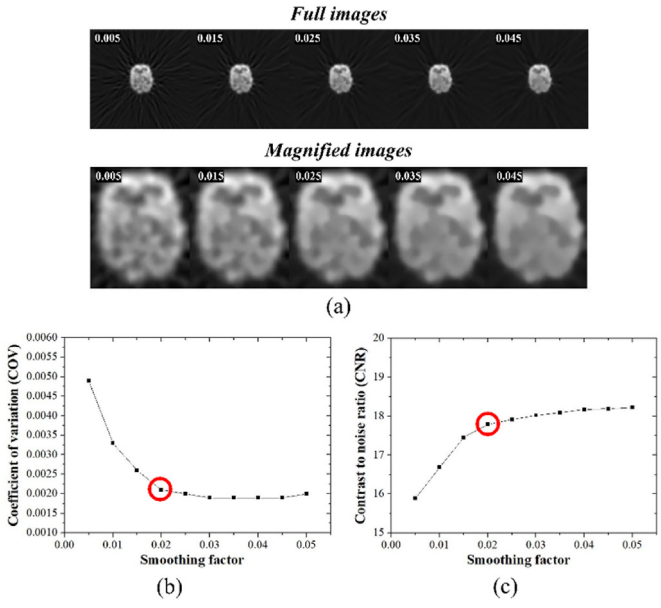

Fig. 2. (a) Result images, (b) COV graph, and (c) CNR graph according to the change in the smoothing factor of the NLM noise reduction algorithm based on the FBP reconstruction method.

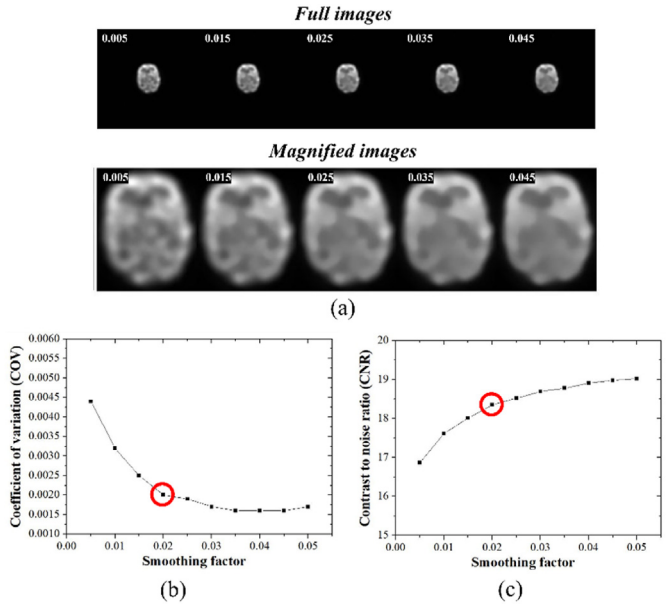

Fig. 3. (a) Result images, (b) COV graph, and (c) CNR graph according to the change in the smoothing factor of the NLM noise reduction algorithm based on the OSEM reconstruction method.

Fig. 3 shows the results according to the smoothing factor change of the NLM noise reduction algorithm in the brain SPECT image using the OSEM reconstruction method. Fig. 3 (a) shows a SPECT image obtained by changing the smoothing factor of the NLM noise reduction algorithm and shows a full-size image and an enlarged image of the brain area. In addition, graphs of the results of the COV and CNR according to the smoothing factor measured in Fig. 3 (a) images are shown in Fig. 3 (b) and (c), respectively. Similarly to the FBP results, we confirmed that the COV results of the OSEM reconstruction image gradually decreased as the smoothing factor increased. When a smoothing factor of 0.005 was used, the COV value was 0.0044 and was 0.0017 when using a smoothing factor of 0.050. When the NLM noise reduction algorithm with a smoothing factor of 0.020 was applied to the SPECT image, a COV of 0.0020 was derived, similar to the result measured with a smoothing factor of 0.050. In addition, we confirmed that the COV results of the OSEM reconstruction image gradually decreased as the smoothing factor increased, with the same tendency as the evaluation result using the FBP reconstruction method. When a smoothing factor of 0.005 was used, the CNR value was measured to be 16.87, which was confirmed to be 19.02 with a smoothing factor of 0.050. When the NLM noise reduction algorithm with a smoothing factor of 0.020 was applied to the SPECT image, the CNR of 18.35 was derived, showing that it was similar to the result measured with a smoothing factor of 0.050. We showed that applying the NLM noise reduction algorithm with a smoothing factor of 0.020 to the brain SPECT image based on the OSEM reconstruction method is the optimal value because the slope change of the COV and CNR result graphs starts to become almost constant, with the same tendency as the evaluation result using the FBP reconstruction method.

In brain SPECT images using the FBP and OSEM reconstruction methods, the NLM noise reduction algorithm using a 0.020 smoothing factor was the most efficient. To prove the noise removal efficiency of the image to which the optimal NLM algorithm was applied, a comparative evaluation was performed by modeling the conventional filtering method. Fig. 4 shows the results of applying

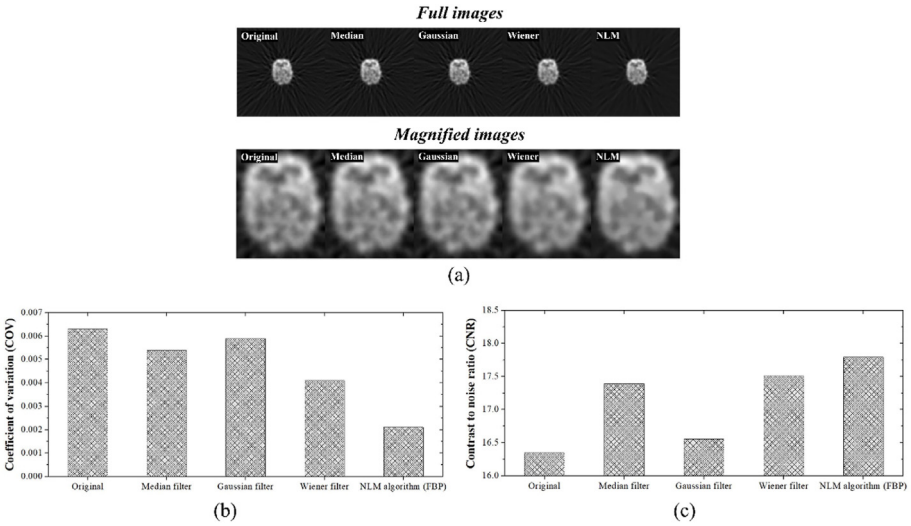

Fig. 4. Comparison results between the NLM noise reduction algorithm applied with the optimal smoothing factor of 0.020 based on the FBP reconstruction method and the conventional filtering methods: (a) result images, (b) COV graph, and (c) CNR graph.

various filtering methods and the optimal NLM noise reduction algorithm to the brain SPECT image using the FBP reconstruction method. Fig. 4 (a) shows the SPECT image obtained using FBP reconstruction for each noise reconstruction method, and the obtained COV and CNR result graphs are shown in Fig. 4 (b) and (c). The COV values of the original image, median filter, Gaussian filter, Wiener filter, and optimized NLM algorithm in the SPECT image acquired using FBP reconstruction were 0.0063, 0.0054, 0.0059, 0.0041, and 0.0021, respectively. The COV values of the SPECT image with FBP reconstruction using the optimized NLM algorithm were 66.67%, 66.11%, 64.41%, and 48.78% higher than those of the original image, median filter, Gaussian filter, and Wiener filter, respectively. In addition, the CNR values of the original image, median filter, Gaussian filter, Wiener filter, and optimized NLM algorithm in the SPECT image acquired using FBP reconstruction were derived as 16.35, 17.39, 16.55, 17.51, and 17.79, respectively. The CNR results of the SPECT image with FBP reconstruction using the optimized NLM algorithm were 8.81%, 2.30%, 7.49%, and 1.60% higher than those of the original image, median filter, Gaussian filter, and Wiener filter, respectively. Fig. 5 shows the results of applying various filtering methods and the optimal NLM noise reduction algorithm to the brain SPECT image using the OSEM reconstruction method. Fig. 5 (a) shows the SPECT image obtained using OSEM reconstruction for each noise reconstruction method, and the obtained COV and CNR result graphs are shown in Fig. 5 (b) and (c). The COV values of the original image, the median filter, Gaussian filter, Wiener filter, and optimized NLM algorithm in the acquired SPECT image using OSEM reconstruction were derived as 0.0061, 0.0051, 0.0059, 0.0036, and 0.0020, respectively. The COV results of the SPECT image with OSEM reconstruction using the optimized NLM algorithm were 67.21%, 60.78%, 66.10%, and 44.44% higher than those of the original image, median filter, Gaussian filter, and Wiener filter, respectively. Moreover, the CNR values of the original image, median filter, Gaussian filter, Wiener filter, and optimized NLM algorithm in the acquired SPECT images using OSEM reconstruction were derived as 17.12, 17.79, 17.43, 18.13, and 18.35, respectively. The CNR results of the SPECT image with OSEM reconstruction using the optimized NLM algorithm were 7.18%, 3.15%, 5.28%, and 1.21%

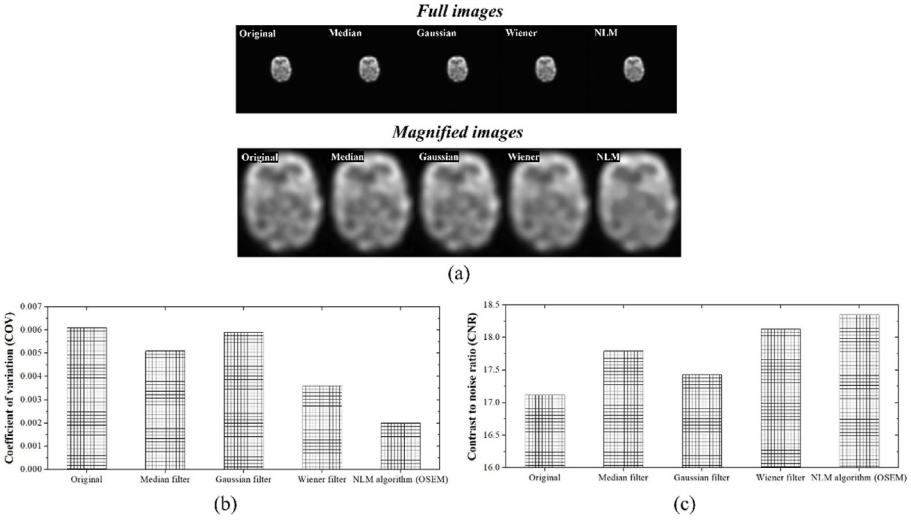

Fig. 5. Comparison results between the NLM noise reduction algorithm applied with the optimal smoothing factor of 0.020 based on the OSEM reconstruction method and the conventional filtering methods: (a) result images, (b) CNR graph, and (c) COV graph.

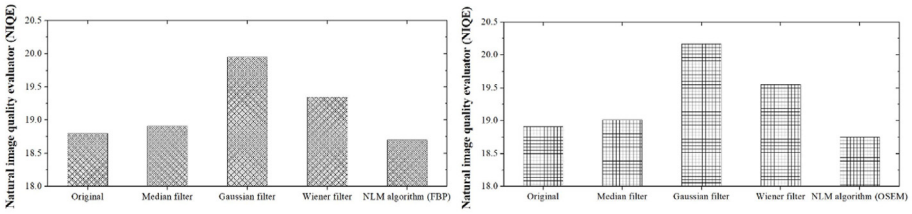

Fig. 6. Plot of the natural image quality evaluator (NIQE) corresponding to the NLM noise reduction algorithm with the optimal smoothing factor of 0.020 and conventional filtering methods in the brain SPECT image using (a) FBP and (b) OSEM reconstructions.

higher than those of the original image, median filter, Gaussian filter, and Wiener filter, respectively.

In this study, the COV and CNR results of the optimized NLM noise reduction algorithm in the brain SPECT phantom image using the FBP and OSEM reconstruction methods improved by approximately 66.94 and 8.00%, respectively, compared to the original image. Although COV and CNR are the parameters that can analyze the noise level more accurately, it is difficult to evaluate the blurring effect in SPECT images. Reducing noise in brain SPECT images due to the use of a small number of gamma-ray photons is a key point in nuclear medicine, but the ability to enhance or preserve edge regions is also important. *Kim* et al. emphasized the importance of simultaneously improving noise and blurring in gamma camera images and analyzed the results using the intensity profile [16]. However, because the profile has limitations in quantitatively observing the noise and blurring distribution, no-reference-based image quality evaluation has been widely used in recent years. *Mittal* et al. proposed a no-reference evaluation model that can analyze completely blind image quality, and the opinion-unaware natural image quality evaluator (NIQE) evaluation parameter is being applied in various ways for complex image quality evaluation in the medical imaging field [17]. In this study, the NIQE evaluation parameter was used and compared with conventional methods to observe the overall quality improvement of the NLM noise reduction algorithm in brain SPECT images. Fig. 6 (a) and (b) are graphs of the NIQE results obtained by applying the noise reduction method to brain SPECT images based on the FBP and OSEM reconstruction methods, respectively. The NIQE values of the original image, median filter, Gaussian filter, Wiener filter, and optimized NLM algorithm in the acquired SPECT images using FBP reconstruction were derived as 18.80, 18.91, 19.95, 19.35, and 18.70, respectively. Furthermore, the NIQE values of the original image, median filter, Gaussian filter, Wiener filter, and optimized NLM algorithm in the acquired SPECT images using OSEM reconstruction were derived as 18.91, 19.01, 20.17, 19.55, and 18.78, respectively. In the results of the FBP and OSEM reconstruction methods, the NIQE value of the SPECT image to which the NLM noise reduction algorithm was applied was superior to that of the original image. Based on the NIQE results, the NLM noise reduction algorithm applied with the optimized smoothing factor was expected to reduce the noise level while preserving the edge area in the brain SPECT image as much as possible.

In the future, we intend to study the applicability of noise reduction algorithms based on various reconstruction methods that can be used when acquiring brain SPECT images. In the FBP reconstruction method, the image characteristics change depending on the filter used. In the iterative reconstruction method, the image quality changes based on the number of iterations or subsets. When acquiring brain SPECT images, the parameters of the NLM noise reduction algorithm optimized according to the reconstruction method are derived and the characteristics are analyzed so that various applications in the field of nuclear medicine are possible. In addition, we intend to further consider improving the image processing speed, which is the main problem of NLM approach.

Deep learning or machine learning techniques are actively used in medical image denoising algorithms [18–20]. In photoacoustic images, artificial intelligence technology using various learning structures is used as a noise reduction method [18], and in particular, the usefulness of convolutional neural networks is being proven in many fields [19]. Recently, the possibility of application in myocardial perfusion imaging has improved as *Olia* et al. proposed a deep learning framework for noise removal in SPECT images with low dose applied [20]. In addition, deep learning technology is widely used in bone age estimation using X-ray images, fields using magnetic resonance imaging, prediction of Parkinson's disease progression, and metal artifact reduction in dental computed tomography [21–24]. In the future, these artificial intelligence technologies are expected to be fused with noise reduction algorithms and applied in various methods.

4. Conclusion

This study demonstrates the usefulness of the NLM noise reduction algorithm for brain SPECT images based on various reconstruction methods. We hope the proposed NLM algorithm can be used more effectively in SPECT images with relatively high noise levels than in other medical images.

Declaration of competing interest

The authors declare that they have no known competing financial interests or personal relationships that could have appeared to influence the work reported in this paper.

.

Acknowledgments

This work was supported by the Gachon University research fund of 2022 (GCU-202206110001) and was supported by the National Research Foundation of Korea (NRF-2021R1F1A1061440). We would like to thank Yongho Do who works at Seoul Metropolitan Government Seoul National University Boramae Medical Center for helping us acquire SPECT data.

References

[1] H.H. Park, T.H. Kim, J.Y. Shin, T.S. Lee, K.Y. Lyu, Usefulness of CT based SPECT fusion image in the lung disease: preliminary study, J. Radiol. Sci. Technol. 35 (2012) 59–64.
[2] T. Yamamoto, J.M. Kim, K.S. Lee, T. Takayama, T. Kitahara, Development of a new cardiac and Torso phantom for verifying the accuracy of myocardial perfusion SPECT, J. Radiol. Sci. Technol. 31 (2008) 389–399.
[3] W. Zheng, S. Li, A. Krol, C.R. Schmidtlein, X. Zeng, Y. Xu, Sparsity promoting regularization for effective noise suppression in SPECT image reconstruction, Inverse Probl. 35 (2019), 115011.
[4] D.G. Amen, M. Trujillo, A. Newberg, K. Willeumier, R. Tarzwell, J.C. Wu,

B. Chaitin, Brain SPECT imaging in complex psychiatric cases: an evidence-based, underutilized Tool, Open Neuroimaging J. 5 (2011) 40–48.
[5] N.A. Nikolov, S.S. Makeev, O. Korostynska, T.G. Novikova, Y.S. Kriukova, Gaussian filter for brain SPECT imaging, Int. Biosyst. and Bioeng. 6 (2022) 4–15.
[6] P.P. Bruyant, Analytic and iterative reconstruction algorithms in SPECT, J. Nucl. Med. 43 (2002) 1343–1358.
[7] S. Vandenberghe, Y. D'Asseler, R. Van de Walle, T. Kauppinen, M. Koole, L. Bouwens, K. Van Laere, I. Lemahieu, R.A. Dierckx, Iterative reconstruction algorithms in nuclear medicine, Comput. Med. Imag. Graph. 25 (2001) 105–111.
[8] A.C. Trevisan, M.D. Raed, V. Tumas, L. Alexandre-Santos, F.A. Pitella, E.N. Itikawa, J.H. Silvah, M. Kato, E.Z. Martinez, J.A. Achcar, M.V. Simoes, L. Wichert-Ana, Comparison between OSEM and FBP reconstruction algorithms for the qualitative and quantitative interpretation of brain DAT-SPECT using an anthropomorphic striatal phantom: implications for the practice, Res. on Biomed. Eng. 36 (2020) 77–88.
[9] L.I. Ruudin, S. Osher, E. Fatemi, Nonlinear total variation based noise removal algorithms, Physica D 60 (1992) 259–268.
[10] H.V. Bhujle, B.H. Vadavadagi, NLM based magnetic resonance image denoising – a review, Biomed. Signal Process Control 47 (2019) 252–261.
[11] B.G. Kim, S.H. Kang, C.R. Park, H.W. Jeong, Y. Lee, Noise level and similarity analysis for computed tomographic Thoracic image with fast non-local means denoising algorithm, Appl. Sci. 10 (2020), https://doi.org/10.3390/app10217455.
[12] M.Y. Jang, C.R. Park, S.H. Kang, Y. Lee, Experimental study of the fast non-local means noise reduction algorithm using the Hoffman 3D brain phantom in nuclear medicine SPECT image, Optik 224 (2020), 165440.
[13] S.H. Kang, J.Y. Kim, Application of fast non-local means algorithm for noise reduction using separable color channels in light microscopy images, Int. J. Environ. Res. Publ. Health 18 (2021), https://doi.org/10.3390/ijerph18062903.
[14] A. Buades, B. Coll, J.M. Morel, A Non-local Algorithm for Image Denoising, IEEE Computer Society Conference on Computer Vision and Pattern Recognition (CVPR'05), 2005, https://doi.org/10.1109/CVPR.2005.38.
[15] D. Choi, S.H. Kang, C.R. Park, Y. Lee, Study of the noise reduction algorithm with median modified wiener filter for T2-weighted magnetic resonance brain images, J. of Magn. 26 (2021) 50–59.
[16] K. Kim, M.H. Lee, Y. Lee, Investigation of a blind-deconvolution framework after noise reduction using a gamma camera in nuclear medicine imaging, Nucl. Eng. Technol. 52 (2020) 2594–2600.
[17] A. Mittal, R. Soundararajan, A.C. Bovik, Making a "completely blind" image quality analyzer, IEEE Signal Process. Lett. 20 (2013) 209–212.
[18] P. Rajendran, A. Sharma, M. Pramanik, Photoacoustic imaging aided with deep learning: a review, Biomed. Eng. Letters 12 (2022) 155–173.
[19] L. Gondara, Medical Image Denoising Using Convolutional Denoising Autoencoders, 2016 IEEE 16th International Conference on Data Mining Workshops (ICDMW), 2017, https://doi.org/10.1109/ICDMW.2016.0041.
[20] N.A. Olia, A. Kamali-Asl, S.H. Tabrizi, P. Geramifar, P. Sheikhzadeh, S. Farzanefar, H. Arabi, H. Zaidi, Deep learning–based denoising of low-dose SPECT myocardial perfusion images: quantitative assessment and clinical performance, Eur. J. Nucl. Med. Mol. Imag. 49 (2022) 1508–1522.
[21] J.H. Lee, Y.J. Kim, K.G. Kim, Bone age estimation using deep learning and hand X-ray images, Biomed. Eng. Letters 10 (2020) 323–331.
[22] C. Wright, P. Makela, A. Bigot, M. Anttinen, P.J. Bostrom, R.B. Sequeiros, Deep learning prediction of non-perfused volume without contrast agents during prostate ablation therapy, Biomed. Eng. Letters (2022), https://doi.org/10.1007/s13534-022-00250-y.
[23] A.H. Shahid, M.P. Singh, A deep learning approach for prediction of Parkinson's disease progression, Biomedical Engineering Letters 10 (2020) 227–239.
[24] M.A.A. Hegazy, M.H. Cho, M.H. Cho, S.Y. Lee, U-net based metal segmentation on projection domain for metal artifact reduction in dental CT, Biomed. Eng. Letters 9 (2019) 375–385.